Dependence of surface atomic arrangement of titanium dioxide on metallic nanowire nucleation by thermally assisted photoreduction

Hsien-Tse Tung,[a] Jenn-Ming Song,[b] Shih-Wei Feng,[c] Changshu Kuo[a] and In-Gann Chen*[a]

Received 29th September 2009, Accepted 4th November 2009
First published as an Advance Article on the web 30th November 2009
DOI: 10.1039/b920150e

Through studying the optical, electrical and photocatalytic properties of anatase TiO_2 films with different preferred orientations, (101) and (004), this study clarified the relationship between the formation of metallic nanowires by thermally assisted photoreduction process and surface atomic bonding conditions of TiO_2. Experimental results show that the (101) anatase films which yielded much more Ag nanowires than the (004) oriented films and exhibited more complex superficial atomic bonding, which could be demonstrated by the Gaussian bands in photoluminescence spectra. This might lead to higher carrier concentration and mobility, as well as longer life time for photo-exited electrons and consequently a greater photocatalytic activity for reducing metallic ions. The fact that the anatase (101) surface acted as the preferred nucleation sites for Ag nanowires was supported by high resolution transmission electron microscopy lattice image of a TiO_2 nanofiber where an Ag nanowire was grown.

Introduction

TiO_2, a wide band gap oxide semiconductor, has attracted much interest due to its unique properties, such as its high dielectric constant,[1] high refractivity,[2] photocatalysis,[3–6] and super-hydrophilicity.[7] In comparison to the other crystalline phases of TiO_2, anatase is the most photoactive.[8] Its enhanced photoactivity results from the difference in energy band structure.[9] The most stable and frequently observed anatase films have a (101) preferentially oriented structure.[10,11] Investigations on surface science have yielded an abundance of atomic-scale structural and chemical information on anatase (101),[12] whereas works on other anatase planes are scarce,[13,14] probably because of the high surface energy required for growing other oriented planes.

Taking advantage of its photocatalytic capability, anatase TiO_2 is an excellent choice for reducing metal ions from solution by ultraviolet illumination.[15,16] Most often it has been used in the form of nanoparticles for reducing metal ions in solution.[17,18] Notably, one recent breakthrough consisted of the synthesis of various metallic nanowires including Au, Ag, and Cu in large quantities by a modified photoreduction process employing anatase TiO_2, namely thermally assisted photoreduction.[19–21] It has been demonstrated that the crystallinity, surface morphology, and the photocatalytic ability of the anatase TiO_2 substrate significantly influences the yield (or nucleation) of metallic nanowires.

By means of radio-frequency-sputtering and electron-beam-evaporation techniques, anatase films with different preferred orientations of (101) and (004) were obtained respectively in this study for clarifying the relationship between the crystal orientation and physical properties such as the electrical and optical properties, as well as photocatalytic activity. In addition, to further investigate how the crystal structure affects the nucleation of the thermally assisted photoreduced metallic nanowires, an Ag nanowire grown on a TiO_2 fiber prepared by the novel electrospinning process was also examined. Silver nitrate ($AgNO_3$) aqueous solution was chosen as the precursor for forming Ag nanowires.

Materials and methods

Synthesis

The TiO_2 thin films with a thickness of 400 ± 30 nm were prepared by radio-frequency-sputtering and electron-beam-evaporation techniques on 1 cm^2 square silicon wafers. For the radio-frequency-sputtering method, evacuation was done using a turbomolecular pump (Alcatel ATP400) to a base pressure lower than 5×10^{-6} Torr and the deposition was proceeded in a mixed atmosphere of argon (99.99%) and oxygen (99.99%) gases. The circular magnetron equipped with a titanium target (Solar Comp., 99.9%) was powered by a radio frequency supply operating at a frequency of 13.56 MHz and a constant power of 300 Watts. The electron-beam-evaporation method was evacuated by a mechanical pump (Alcatel 2033SD) and a cryopump (Cti-Cryo-Torr8) to a base pressure lower than 10^{-6} Torr. A TiO_2 (Solar Comp., 99.9%) target was used and the films were deposited in oxygen atmosphere. The TiO_2 electro-spun nanofibers were prepared by mixing with 3 mL of acetic acid (Aldrich, 99%) and 3 mL of ethanol (Aldrich, ≥ 99%), followed by the drop wise addition

[a] *No. 1, University Road, Tainan 70101, Taiwan. E-mail: ingann@mail.ncku.edu.tw; Fax: +886 6 238 1695; Tel: +886 6 276 3741*
[b] *No.1, Sec. 2, Da Hsueh Road, Hualien 97401, Taiwan. E-mail: samsong@mail.ndhu.edu.tw; Tel: +886 3 863 4605*
[c] *700, Kaohsiung University Rd., Nanzih District, 811. Kaohsiung, Taiwan. E-mail: swfeng@nuk.edu.tw; Fax: +886 7 5919357; Tel: +886 7 5919354*

of 3 g of titanium isopropoxide (Aldrich, 97%) precursors. The polymer-based sol–gel solution was completed by adding a solution containing 0.42 g of polyvinylpyrrolidone with molecular weight of 40 000 (Aldrich, 99.5%) and 8 mL of ethanol and was loaded in a syringe equipped with a 21 gauge stainless needle. The high voltage source of up to 15 kV connected to the flat tip needle and a jet formed resulting in fibers deposited on the Au grid target. All the above-mentioned TiO_2 products obtained were heated at 500 °C, followed by an isothermal stage at 500 °C for 8 h to transform to the anatase phase.

To produce Ag nanowires, 15 μL droplets of 0.1 M $AgNO_3$ aqueous solution were dropped on the annealed TiO_2 substrate (including thin films and electrospinning nanofibers), which were placed on quartz plates and heat treated in an infrared furnace in air. The samples were heated up at a constant rate of 5 °C per min, followed by an isothermal stage at 300 °C for 3 h and finally furnace-cooled to the ambient temperature. In order to prepare the TEM sample, the Ag nanostructures were separated from the TiO_2 substrate by ultrasonication for 10 min in ethanol and subsequently dropped the ethanol with Ag nanowires on the Cu grid.

Characterization

The structure and preferred orientation of TiO_2 were characterized using X-ray diffraction (XRD, Rigaku D/MAX2500), scanning electron microscope (SEM, EVO50), energy dispersive spectroscopy (EDS, JSM-7000) and transmission electron microscopy (TEM, JEM-2100F). The electrical properties of TiO_2 films were examined by van der Pauw Hall measurements at room temperature. The optical properties of the TiO_2 films were investigated by using photoluminescence (PL) and time-resolved photoluminescence (TRPL). The PL measurements were carried out at 10 K with the 325 nm line of a 35 mW helium–cadmium laser for excitation. The TRPL measurements, which were performed using a Hamamatsu streak camera with a time resolution of about 5 ps. The photocatalytic capability of TiO_2 films were evaluated by measuring the contact angle between 15 μL water droplets and the surface of 1 cm^2 square TiO_2 substrate, all of which were performed in ambient atmosphere (65% humidity) at room temperature (20 °C). The samples were first exposed under a halogen lamp (8 mW cm^{-2} at 360 nm) for 48 h and stored in the dark. The change in the contact angle was recorded up to a storage time of 336 h.

Results and discussion

Characteristics of TiO_2 films with respect to crystalline orientation

The preferred orientations of the TiO_2 films prepared by radio-frequency-sputtering and electron-beam-evaporation were demonstrated by the grazing angle X-ray diffraction patterns (Fig. 1). As illustrated, the radio-frequency-sputtering films are (101) oriented polycrystalline anatase, while the electron-beam-evaporation films showed a strong (004) preferred orientation. The AFM images of the above TiO_2 substrates with different surface orientations were shown in

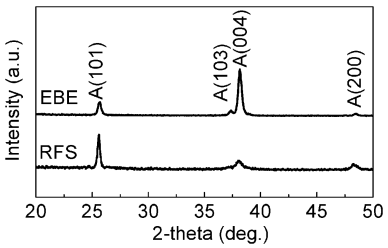

Fig. 1 XRD patterns of TiO_2 thin films annealed at 500 °C for 8 h with (lower) (101) and (upper) (004) preferentially oriented structures.

Fig. 2. The average surface roughnesses of the samples did not differ too much, which were 1.6 nm for (101) oriented films and 2.5 nm for (004) oriented films. Table 1 lists the results of the Hall measurement. It was found that both samples were n-type semiconductors. The carrier concentration and mobility of the anatase (101) oriented films were higher than those of the anatase (004). In contrast, the (004) oriented films exhibited a greater electrical resistivity.

With respect to the optical properties, Fig. 3(a) and (b) illustrate the photoluminescence spectra of the (101) and (004) oriented TiO_2 films measured at 10 K respectively. It is known that the free excitonic emission diminishes as the temperature goes down.[22–24] Instead, some narrower peaks, originating from the exciton bound at either the donor or acceptor, appear at cryogenic temperatures. The PL spectrum in Fig. 3(a) shows that in the case of (101) oriented TiO_2 films, four bands with peaks at 2.36 eV, 2.43 eV, 2.49 eV, and 2.52 eV can be distinguished from the Gaussian distribution based on the literature.[25–27] In comparison, the spectrum of the (004) oriented TiO_2 films (Fig. 3(b)) exhibited a broader luminescence peak comprising two Gaussian bands centered at 2.36 eV and 2.46 eV.

Fig. 4 shows the time-resolved photoluminescence (TRPL) curves of the anatase films. A two-exponential function equation, $I(t) = A_1*\exp(-t/\tau_1) + A_2*\exp(-t/\tau_2)$, was fitted to the data on PL decay profiles, where τ_1 and τ_2 denote the decay times for the faster and the slower components as illustrated in Table 2, and A_1 and A_2 are the PL amplitudes. Following the previous discussion,[28,29] the slow component (τ_2) originates from the indirect formation of self-trapped exciton[30,31] with trapped electrons whereas the fast component (τ_1) is believed to be due to the direct formation of free electrons and holes. The tendency of the profiles indicates that the growth direction of films significantly affected the PL decay behavior. Compared with (004) films, the PL of the (101) samples took more time to decay, and its fast component

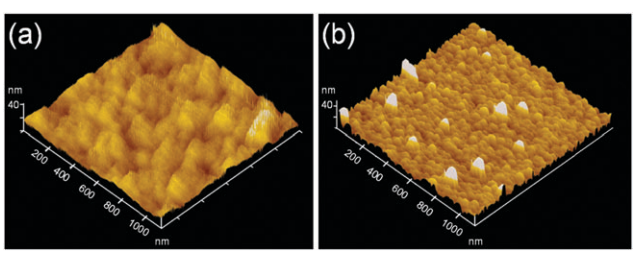

Fig. 2 AFM morphologies of TiO_2 thin films annealed at 500 °C for 8 h with (a) (101) and (b) (004) preferentially oriented structures.

Table 1 Electrical properties obtained from the Hall measurement

Sample	Type	Carrier concentration/cm^{-3}	Mobility/$cm^2\ V^{-1}\ s$	Resistivity/Ω cm
(101) oriented	n	1.99×10^{17}	1092	1.66×10^{-2}
(004) oriented	n	5.24×10^{16}	312	2.27×10^{-1}

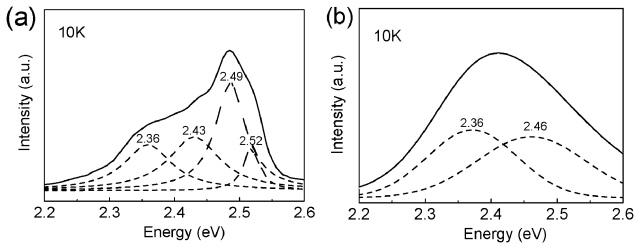

Fig. 3 PL spectra of (a) (101) oriented TiO_2 film and (b) (004) oriented TiO_2 film at 10 K; PL spectra (solid line) are deconvoluted into Gaussian distributions (dashed lines).

(τ_1) reached 82% of a decrease in total. The large fraction of the fast component implies the high concentration of charge carriers for anatase (101) oriented films, which is identical to the results of Hall measurements. Worthy of notice is that the slow component representing the indirect recombination of electron-hole pairs for the (101) oriented film lasted at least two times longer than that for the (004) oriented film. We believe that the PL decay time is strongly affected by the difference in the crystal orientation of superficial bonding. This will be discussed in more detail later.

The photocatalyst hydrophilicity of the samples was also examined. Fig. 5 shows the time dependence of the contact angle (ϕ) of the water drops on the (101) and (004) oriented films in the dark after ultraviolet irradiation. In both the cases, an increase in the contact angle was observed with prolonged storage in the dark, which indicates the degradation of the photocatalytic ability. With the contact angles after a short period of time in the dark (ϕ_S), a long period of time in the dark (ϕ_L), 0 h in the dark (right after UV irradiation) (ϕ_{0h}), and 336 h (14 days) in the dark (ϕ_{336h}), the degradation ratio in contact angle, R_ϕ, can be defined as $(\phi_L - \phi_S)/(\phi_{336h} - \phi_{0h})$. From the fully excited state to the first 96 h in the dark and from then to 336 h, R_ϕ of the (101) oriented film changed from 0.80 to 0.20. This means the contact angles of (101) samples ascended rapidly during the first 96 h, and subsequently the increasing of R_ϕ became slow. The contact angle of (004) samples rose much faster and reached $R_\phi = 0.83$ in the first 48 h. After that, the contact angle of water on (004) oriented films exceeded 30°, while that on the (101) oriented films remained lower than 30° even after 14 days. It can be inferred that the (101) oriented TiO_2 films exhibit a more stable photocatalytic ability, which implies that the photo-excited electrons on the (101) surface have a longer lifetime.

Table 2 Summary of the multi-component exponential curve fitting

Sample	τ_1	τ_2
(101) oriented	0.36 ns (82%)	5.31 ns (18%)
(004) oriented	0.23 ns (44%)	2.08 ns (56%)

Effect of the orientation of TiO_2 on the nucleation of Ag nanowires

The SEM images in Fig. 6(a) and (b) display the Ag nanowires synthesized by heating aqueous $AgNO_3$ droplets respectively on the (101) and (004) oriented TiO_2 films at 300 °C. The Ag nanowires have lengths ranging from 4 μm to 10 μm and a diameter of about 150 nm. The inset of the Fig. 6(b) illustrates that the nanowires showed a pentagonal appearance. The structure of the nanowire was investigated by using transmission electron microscopy (TEM). The diffraction pattern shown in Fig. 6(c) confirms that the Ag nanowire is monocrystalline with a growth direction along [01$\bar{1}$] and no impurities were detected. Interestingly, the population of nanowires on (004) films was significantly lower than that on (101) films and most of the reduced Ag appeared as nodules rather than wires. The chemical analytical results shown in Fig. 6(d) demonstrates that the nanowires were pure Ag without detectable impurities.

To explore the orientation relationship between Ag nanowires and TiO_2, an Ag nanorod grown on a TiO_2 nanofiber was prepared and studied (Fig. 7(a)). The electron diffraction pattern of the nanofiber (Fig. 7(b)) shows distinct diffraction

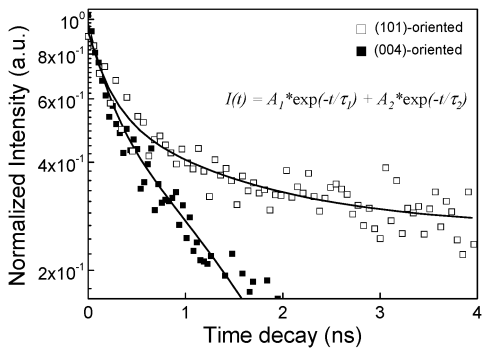

Fig. 4 PL decay profiles of (101) and (004) oriented TiO_2 film.

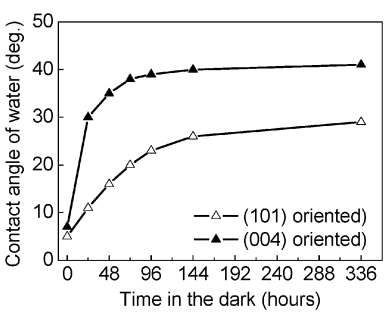

Fig. 5 Variation of the water contact angle in the dark of the (101) and (004) oriented TiO_2 films.

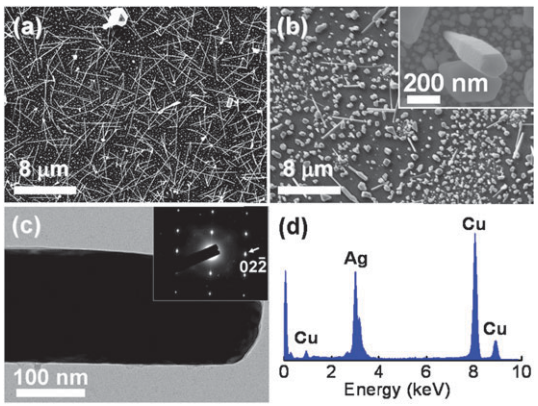

Fig. 6 SEM image of the as-prepared Ag nanowires on (a) (101) oriented and (b) (004) oriented TiO_2 film as well as a higher magnification SEM picture of an isolated Ag nanowire (inset); (c) TEM image of the as-prepared Ag nanowire and its diffraction pattern (inset); (d) the energy dispersive X-ray spectrum of the as-prepared Ag nanowires.

rings corresponding to the (101), (004), and (200) planes of anatase, indicating a fine polycrystalline structure. Fig. 7(c) shows a high-resolution TEM lattice image near a facet of nanofiber on which the Ag nanorod grew. Clear lattice fringes of the (101) planes of the anatase structure with a *d*-spacing of 0.35 nm were identified. This verifies that the anatase (101) plane acted as the preferred nucleation site for Ag nanowires.

Aspect of atomic arrangement and bonding

In order to explain the aforementioned differences between (101) and (004) oriented films, we should consider the atomic arrangement on the surface of anatase films with respect to crystal orientations. As sketched in Fig. 8(a), the surface of (101) oriented TiO_2 film has a sawtooth-like corrugation[12] with fully coordinated six-fold Ti atoms, Ti_{6C}, and three-fold O atoms, (O_{3C}), as well as under-coordinated five-fold Ti, Ti_{5C}, and two-fold O, O_{2C}. Each Ti_{5C} or O_{2C} is deficient in one bonding to oxygen atom or titanium atom. This will form two kinds of defects on the surface of anatase (101). As for the (004) oriented TiO_2 surface (Fig. 8(b)), the atomic model illustrates that the surface is smooth with fully coordinated

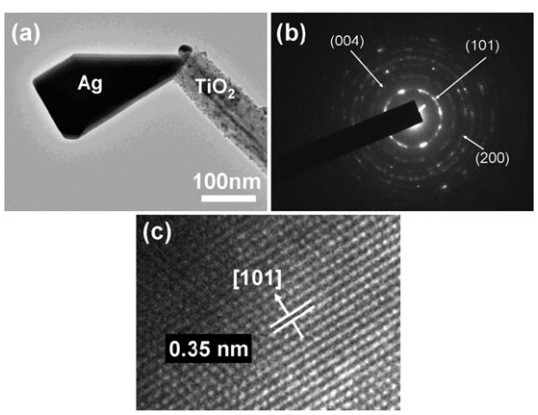

Fig. 7 (a) TEM image of an Ag nanorod grown on an anatase nanofiber; (b) diffraction pattern taken on the anatase nanofiber; (c) HRTEM image of the interfacial region of the anatase nanofiber and Ag nanorod.

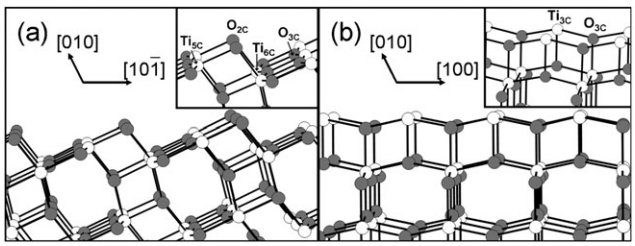

Fig. 8 (a) Atomic model of anatase TiO_2 (101); O atoms are grey, Ti atoms are white; (b) atomic model of anatase TiO_2 (004).

three fold O atoms (O_{3C}) and under-coordinated three-fold Ti atoms (Ti_{3C}) which is deficient in three bonds to oxygen and forms only one kind of surface defect.

The atomic model proposed can also explain the Gaussian distributions in the PL spectra illustrated in Fig. 3. The atoms with various coordination numbers can be ascribed to different Gaussian bands. In the case of the (101) surface, Ti_{6C}, Ti_{5C}, O_{3C}, and O_{2C} correspond to four Gaussian bands; likewise two Gaussian bands in the spectrum of (004) samples represent Ti_{3C} and O_{3C}. Next, considering the TRPL results and the ability to form nanowires, the complex superficial conditions and atomic bonding on the (101) surface might lead to a greater efficiency in trapping charge carriers and thus extend the recombination rate of electron-hole pairs. This can explain the long-lasting photo-excited electrons on the (101) oriented surface and why it serves as the preferential nucleation site for nanowires.

Conclusions

To summarize, the crystal orientation of anatase thin film not only affects its physical properties, but also influences the nanowires forming ability of TiO_2. The TRPL measurements and hydrophilicity test revealed that the photo-excited electrons on the surface of (101) oriented TiO_2 film have longer lifetime than that of the (004) oriented film. This was closely related to the complex bonding conditions of superficial atoms, which could be verified by the numbers of Gaussian bands in the PL spectrum. The advantages in the superficial properties made the anatase (101) films have a greater ability to form Ag nanowires through thermally assisted photoreduction process.

References

1 S. K. Kim, W. D. Kim, K. M. Kim, C. S. Hwang and J. Jeong, *Appl. Phys. Lett.*, 2004, **85**, 4112.
2 M. Zhanga, G. Lina, C. Dong and L. Wen, *Surf. Coat. Technol.*, 2007, **201**, 7252.
3 A. Fujishima and K. Honda, *Nature*, 1972, **238**, 37.
4 H. Ohsaki, N. Kanai, Y. Fukunaga, M. Suzuki, Y. Shibayama, T. Watanabe and K. Hashimoto, *Thin Solid Films*, 2008, **516**, 4558.
5 C. Guillard, D. Debayle, A. Gagnaire, H. Jaffrezic and J. M. Herrmann, *Mater. Res. Bull.*, 2004, **39**, 1445.
6 B. Kim, D. Byun, J. K. Lee and D. Park, *Jpn. J. Appl. Phys.*, 2002, **41**, 222.
7 A. I. Kontos, A. G. Kontos, D. S. Tsoukleris, G. D. Vlachos and P. Falaras, *Thin Solid Films*, 2007, **515**, 7370.
8 P. Zeman and S. Takabayashi, *Thin Solid Films*, 2003, **433**, 57.
9 A. L. Linsebigler, G. Lu and J. T. Yates, *Chem. Rev.*, 1995, **95**, 735.
10 U. Diebold, N. Ruzycki, G. S. Herman and A. Selloni, *Catal. Today*, 2003, **85**, 93.

11 V. Shklover, M. K. Nazeeruddin, S. M. Zakeeruddin, C. Barbé, A. Kay, T. Haibach, W. Steurer, R. Hermann, H. U. Nissen and M. Grätzel, *Chem. Mater*., 1997, **9**, 430.
12 X. Q. Gong, A. Selloni, M. Batzill and U. Diebold, *Nat. Mater*., 2006, **5**, 665.
13 S. Yamamoto, T. Sumita, Sugiharuto, A. Miyashita and H. Naramoto, *Thin Solid Films*, 2001, **401**, 88.
14 T. S. Yang, C. B. Shiu and M. S. Wong, *Surf. Sci*., 2004, **548**, 75.
15 M. R. Hoffmann, S. T. Martin, W. Y. Choi and D. W. Bahnemann, *Chem. Rev*., 1995, **95**, 69.
16 S. Nishimoto, B. Ohtani, H. Kajiwara and T. Kagiya, *J. Chem. Soc., Faraday Trans. 1*, 1983, **79**, 2685.
17 M. I. Litter, *Appl. Catal., B*, 1999, **23**, 89.
18 M. R. V. Sahyun and N. Serpone, *Langmuir*, 1997, **13**, 5082.
19 H. T. Tung, J. M. Song, T. Y. Dong, W. S. Hwang and I. G. Chen, *Cryst. Growth Des*., 2008, **8**, 3415.
20 H. T. Tung, J. M. Song, Y. T. Nien and I. G. Chen, *Nanotechnology*, 2008, **19**, 455603.
21 H. T. Tung, I. G. Chen, J. M. Song and C. W. Yen, *J. Mater. Chem*., 2009, **19**, 2386.
22 P. Zu, Z. K. Tang, G. K. L. Wong, M. Kawasaki, A. Ohtomo, H. Koinuma and Y. Segawa, *Solid State Commun*., 1997, **103**, 459.
23 Z. K. Tang, G. K. L. Wong, P. Zu, M. Kawasaki, A. Ohtomo, H. Koinuma and Y. Segawa, *Appl. Phys. Lett*., 1998, **72**, 3270.
24 R. E. Sherriff, D. C. Reynolds, D. C. Look, B. Jogai, J. E. Hoelscher, T. C. Collins, G. Cantwell and W. C. Harsch, *J. Appl. Phys*., 2000, **88**, 3454.
25 W. F. Zhang, M. S. Zhang, Z. Yin and Q. Chen, *Appl. Phys. B: Lasers Opt*., 2000, **70**, 261.
26 R. Janes, M. Edge, J. Rigby, D. Mourelatou and N. S. Allen, *Dyes Pigm*., 2001, **48**, 29.
27 M. M. Rahman, K. M. Krishna, T. Soga, T. Jimbo and M. Umeno, *J. Phys. Chem. Solids*, 1999, **60**, 201.
28 H. Tang, H. Berger, P. Schmid, F. Lévy and G. Burri, *Solid State Commun*., 1993, **87**, 847.
29 H. Tang, F. Lévy, H. Berger and P. E. Schmid, *Phys. Rev. B: Condens. Matter*, 1995, **52**, 7771.
30 R. Leonelli and J. L. Brebner, *Phys. Rev. B: Condens. Matter*, 1986, **33**, 8649.
31 M. Watanabe, T. Hayashi, H. Yagasaki and S. Sasaki, *Int. J. Mod. Phys. B*, 2001, **15**, 3997.

